6052 *Biochemistry* **2010,** *49,* 6052–6063
DOI: 10.1021/bi1006942

BIOCHEMISTRY
including biophysical chemistry & molecular biology
Article

Role of Heme in the Unfolding and Assembly of Myoglobin[†]

David S. Culbertson and John S. Olson*

Department of Biochemistry and Cell Biology and W. M. Keck Center for Computational Biology, Rice University, Houston, Texas 77005

Received May 4, 2010; Revised Manuscript Received June 8, 2010

ABSTRACT: The unfolding of wild-type holomyoglobin in the ferric state (metMb) appears to be a simple two-state process, even though hemichrome spectra are often observed and apoMb denaturation involves an intermediate. To resolve these discrepancies, we measured GuHCl-induced, equilibrium unfolding of five sperm whale metMb variants, which were selected to examine the relative importance of apoglobin stability and hemin affinity. Combined analysis of CD, Trp fluorescence, and Soret absorbance titration curves for all the variants requires a six-state mechanism containing native (N), intermediate (I), and unfolded (U) states of apoMb and their hemin-bound counterparts, NH (holoMb), IH, and UH, respectively. The unfolding parameters for the apoMbs were obtained in independent experiments and then fixed in the analysis of the holoprotein data, where only the affinities of the apoglobin states for hemin were allowed to vary. This cofactor binding analysis applies generally to all globins and led to three specific conclusions. (1) The stability of holo-metMb is determined primarily by the high affinity ($K_d \sim 10^{-13}$ M) of native apoMb (N) for hemin. (2) The partially unfolded intermediate with hemin bound (IH) has a hemichrome spectrum indicative of a bis-histidyl axial coordination and is seen clearly when the stability of the N state or its affinity for hemin is reduced. (3) Although the affinity of the intermediate for hemin ($K_d \sim 10^{-11}$ M) is ~100-fold lower than that for the native state, free hemin can bind to it and promote the assembly of the holoprotein.

For the past 50 years, mammalian myoglobin (Mb)[1] has served as the key model system for structure−function studies of 3-on-3 helical globins (*1*−*4*). The cofactor in native Mb is a type *b* heme (iron-protoporphyrin IX ring), which is directly coordinated to the protein by the proximal histidine side chain (His93 in Mb). The second axial ligand is either exogenous water in the ferric state or O_2 when the iron is reduced, and both of these ligands are indirectly attached to the protein by hydrogen bonding to the distal histidine (His64 in Mb) (*5*). Studies on Mb folding have focused mainly on characterizing the stabilities and structures of initial, intermediate, and final apoglobin states in the absence of heme. Sperm whale apoMb has been shown to lose a significant amount of secondary structure after heme removal, which involves primarily unfolding of the F helix and surrounding EF and FG loops (*6*−*8*). Further perturbation induced by the addition of heat or chemical denaturants (acid, urea, or GuHCl) leads to the complete loss of secondary and tertiary structure.

The existence of a folding intermediate (I) for apoMb was first proposed by Balestrieri et al. (*9*) on the basis of previous steady-state fluorescence experiments by Kirby and Steiner (*10*) and has since been verified by multiple techniques using acid, urea, and guanidine hydrochloride (GuHCl) denaturation (*8*, *11*−*16*). Studies involving rapid jumps from high denaturant concentrations to dilute conditions have demonstrated the presence of a kinetic intermediate, formed within a few milliseconds, that already possesses structure in helices A, G, and H (*17*). Depending on experimental conditions, another kinetic intermediate can be generated along folding pathway (*18*), which has additional structure occurring mostly in helix B (*17*, *19*, *20*). The structures of the equilibrium and kinetic intermediates of apoMb appear to be very similar (*8*, *17*), and only recently have small disparities been found, notably in the E helix (*19*).

In contrast to apoMb, only a few studies have focused on the holoprotein. Most unfolding analyses of intact Mb have been semiempirical, assuming an apparent two-state equilibrium and/or kinetic mechanism (*21*−*27*). Attempts were made to correlate melting temperatures of holoMb empirically with surface electrostatics and folding motifs seen in the crystal structures (*24*−*26*). Only a small number of studies attempted to look experimentally for correlations among apoglobin stability, hemin affinity, and holoprotein stability (*12*, *22*, *28*−*30*). Determining the link between these factors is also key to understanding how to optimize heterologous expression yields of recombinant holoMbs and holoHbs in *Escherichia coli* for either research or commercial purposes (*11*, *12*, *31*−*33*).

Our initial studies suggested that resistance of holoMb to unfolding appears to be determined primarily by heme affinity and is affected little by apoMb stability (*29*); however, the analysis was performed using only a simple two-state model. In addition, we made no attempt to take into account hemichrome species, which are often seen under partially denaturing conditions (*34*−*36*). We have now developed and tested a more complete mechanism for holoMb that allows heme binding to all three of the states observed

[†]Supported by U.S. Public Health Service Grants GM 35649 (J.S.O.) and HL 47020 (J.S.O.) and Grant C-612 (J.S.O.) from the Robert A. Welch Foundation. D.S.C. is the recipient of a predoctoral National Institutes of Health Traineeship from Atherosclerosis and Vascular Biology Training Grant T32 HL007812-11GM.

*To whom correspondence should be addressed. Telephone: (713) 348-4762. Fax: (713) 348-5154. E-mail: olson@rice.edu.

[1]Abbreviations: heme, Fe(II)-protoporphyrin IX or a generic name for both oxidation states of the cofactor; hemin, Fe(III)-protoporphyrin IX; Mb, myoglobin; metMb, ferric form of Mb; Hb, hemoglobin; GuHCl, guanidine hydrochloride; WT, wild-type; sw, sperm whale; CD, circular dichroism; PDB, Protein Data Bank.

 Published on Web 06/11/2010

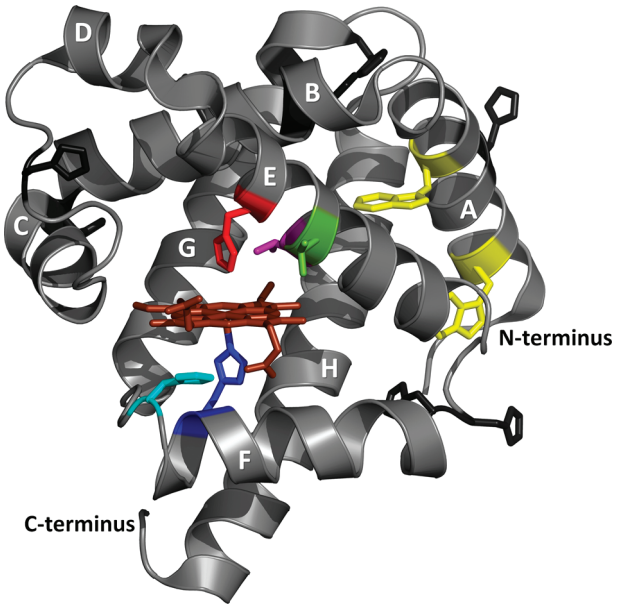

FIGURE 1: Cartoon representation of sperm whale Mb with residues of interest depicted as sticks: His64 (red), Thr67 (green), Val68 (purple), His97 (cyan), His93 (navy blue), and Trp7 and Trp14 (yellow). The other His residues are depicted as black sticks. Helices A−H are labeled in white. Heme is represented as brown sticks. The figure was created using PyMol and PDB entry 1JP6.

during the unfolding of apoMb (i.e., K_d values for hemin binding to the N, I, and U forms) as detailed by Culbertson and Olson (*37*). The affinity of hemin for fully folded, native (N) apoMb is too high to measure directly and is normally estimated from association (*30*, *38*) and dissociation rate constants (*29*, *39*). The K_d for hemin binding to the apoMb N state (K_{NH}) is 10^{-13}−10^{-14} M at neutral pH (*22*, *29*). Hargrove and Olson (*22*) and Robinson et al. (*40*) suggested that hemin can also bind to the completely unfolded states of apoMb and apocytochrome b_{562}, although very weakly with K_{UH} values of $\sim 10^{-6}$ M. However, neither set of authors attempted to measure and characterize heme binding to apoglobin intermediates.

By using a set of five carefully chosen sperm whale metMb variants [i.e., WT, H64F, T67P, V68T, and H97D (Figure 1)], we have been able to demonstrate and characterize heme binding to the apoMb unfolding intermediate. The mutations were selected to stabilize the N apoMb state but weaken hemin affinity (H64F), to selectively destabilize the N state without affecting the hemin affinity or the stability of the I state (T67P), to destabilize the N state but enhance hemin affinity (V68T), and to decrease hemin affinity without affecting the stabilities of the N and I apo states (H97D). Analysis of GuHCl-induced unfolding of these variants requires a six-state mechanism containing native (N), intermediate (I), and unfolded (U) apoMb states and their hemin-bound counterparts, NH (holo-metMb), IH, and UH, respectively. In all of these variants, the apoMb intermediate (I) forms a hemichrome or IH state with a K_d or K_{IH} for hemin binding on the order of $\sim 10^{-11}$ M. This six-state mechanism applies to all monomeric proteins containing noncovalently bound heme with an intermediate regardless of the exact nature of the cofactor-bound intermediate, provides a framework for quantifying the factors that contribute to the overall stability of the holoprotein, and allows an independent and accurate determination of equilibrium constants for hemin binding to native and intermediate apoprotein states.

MATERIALS AND METHODS

Preparation of Proteins. Wild-type sperm whale myoglobin was prepared according to the method of Springer and Sligar (*41*) as modified by Carver et al. (*42*). The H64F and V68T mutant genes were constructed using the cassette mutagenesis system developed by B. A. Springer and K. Egeberg at the University of Illinois (Urbana, IL) (*43*). The T67P and H97D mutants were reconstructed at Rice University for this work using oligonucleotide-directed mutagenesis with a pET29 vector containing the gene for WT Mb to increase yields. All variants were expressed and purified at Rice University following the procedures used for WT Mb, except for the T67P and H97D mutants, which were expressed in *E. coli* BL21-DE3 (Stratagene) and grown at 30 °C for 16−20 h post lag phase in Luria-Bertani medium with 50 μg/mL kanamycin (Sigma). If needed, the protein was purified further using a Superdex-200 gel filtration column (Amersham Biosciences) attached to an FPLC system (Amersham Bio AKTA), and the purity was ≥95% as assessed by SDS−PAGE gels and Soret/280 absorbance ratios. The holoMb concentrations were determined spectroscopically using an ε_{409} of 157 mM^{-1} cm^{-1} for the aquomet forms of WT, T67P, V68T, and H97D Mb (*1*) and with an ε_{393} of 93 mM^{-1} cm^{-1} for the ferric pentacoordinate H64F variant [based upon the CO-bound form at 424 nm using an ε_{424} of 187 mM^{-1} cm^{-1} for all the MbCO samples (*1*)]. ApoMb was prepared using a methyl ethyl ketone extraction method at low pH (*39*, *44*). The resultant apoprotein was then filtered to remove any precipitated protein and used immediately. The concentrations of apoMb variants were determined spectroscopically using an ε_{280} of 15.2 mM^{-1} cm^{-1} (*45*).

Sample Preparation and Spectroscopic Measurements. The samples were prepared using an 8 M stock of guanidine hydrochloride (GuHCl) (Sigma), appropriate amounts of potassium phosphate buffer (Fisher Scientific) to bring the concentration to 10 mM at pH 7, purified Milli-Q water, and concentrated protein. The mixtures were left to equilibrate for 2 h at 20 °C. Spectroscopic measurements were taken on a Jasco 610 instrument for CD, a Varian Cary Eclipse instrument for fluorescence emission, and a Varian Cary 50 instrument for UV−visible absorbance spectra. Each sample chamber was equipped with a Peltier temperature regulator. A reference hemichrome spectrum was generated via addition of high concentrations of imidazole to the ferric myoglobins using a pH-adjusted 1 M stock solution from the powder form (Sigma). To examine the reversibility of hemichrome formation, we rapidly reduced anaerobically metMb samples containing hemichrome intermediates by addition of sodium dithionite (Fluka).

Fitting of ApoMb Equilibrium Unfolding Data. Equilibrium unfolding of the apoMb variants was followed by both far-UV CD and intrinsic fluorescence measurements and analyzed in terms of the three-state mechanism represented in Figure 2. The amount of helical content was analyzed by measuring the ellipticity at 222 nm. Changes in the environment of the Trp side chains were followed by measuring fluorescence emission at 341 nm, which gives rise to a bell-shaped curve with an increase in fluorescence for the intermediate I state and a decrease for the completely unfolded or U state [see Figure 2 (*12*, *15*, *16*)]. This rise and fall of fluorescence intensity allows better definition of the three-state unfolding parameters. The origin of the hyperfluorescence from the intermediate state still remains unclear. The fluorescence of WT apoMb has been suggested to reflect

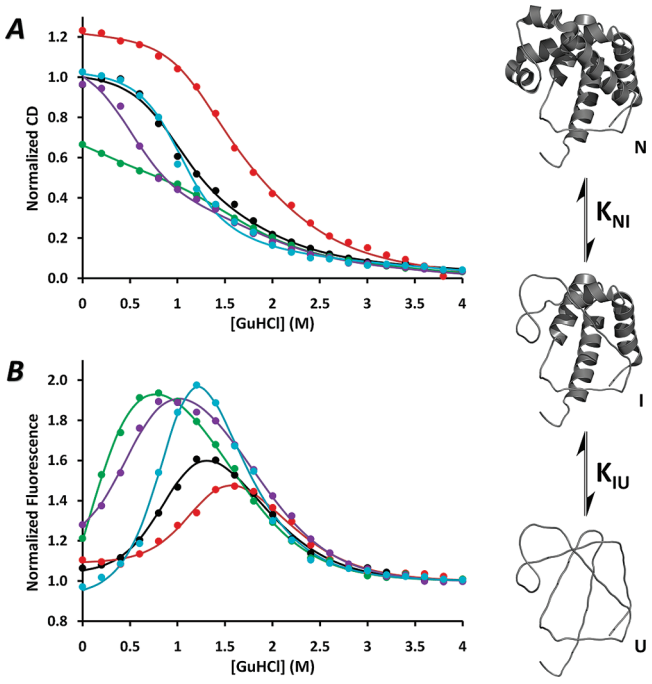

FIGURE 2: GuHCl-induced equilibrium unfolding of apoMb variants. We obtained the unfolding curves by normalizing the changes in far-UV CD at 222 nm to 1.0 for native WT apoMb and assuming that the U states of all five variants have the same CD_{222} and by normalizing fluorescence emission intensities at 341 nm to 1.0 for the final, completely unfolded state of each mutant. Global fits to a three-state mechanism are shown for WT (black), H64F (red), T67P (green), V68T (purple), and H97D (cyan). Conditions: 10 μM protein, 10 mM potassium phosphate buffer, pH 7, 20 °C. The three-state unfolding mechanism is depicted on the right, with the structures of N, I, and U states. The structures were created using PyMol and PDB entry 1JP6 for WT holo-metMb, taking into account the secondary structure present in the N state (*6*−*8*) and in the I state (*8*, *17*). The thick ribbons indicate intact helical secondary structure, and the thin lines represent unfolded structures. The U state is considered completely unfolded.

emission from Trp7 centered at 333 nm, which is quenched by Lys79 in the folded state but not in the intermediate, and emission centered at 321 nm from Trp14, which is buried in the apolar region among the A, G, and H helices in both the N and I states and quenched only after unfolding (*10*, *12*, *46*−*48*). Alternatively, the hyperfluorescence of the intermediate could be caused by the enhanced flexibility of the fluorophores in the intermediate state (*49*).

The equilibrium unfolding curves from far-UV CD and fluorescence data for apoMb variants were fit to a two-step, three-state mechanism, allowing the K_{NI}^0 and K_{IU}^0 equilibrium stability constants for the N-to-I and I-to-U transitions, respectively, to vary. The linear dependencies of the corresponding free energies for the N-to-I and I-to-U transitions on GuHCl concentrations are defined by m_{NI} and m_{IU} values, respectively.

$$K_{NI} = \frac{[I]}{[N]} = K_{NI}^0 \exp\left(\frac{m_{NI}[GuHCl]}{RT}\right) \quad (1)$$

$$K_{IU} = \frac{[U]}{[I]} = K_{IU}^0 \exp\left(\frac{m_{IU}[GuHCl]}{RT}\right) \quad (2)$$

The observed signal at a given GuHCl concentration is the weighted sum of the observable signals, S_N, S_I, and S_U, for each

Scheme 1: Six-State Model for the Unfolding of HoloMb

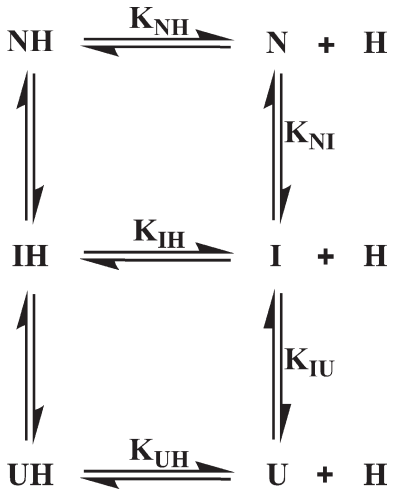

state (*11*, *12*, *14*, *16*), which is expressed as

$$S = \left\{S_N + S_I K_{NI}^0 \exp\left(\frac{m_{NI}[GuHCl]}{RT}\right) + S_U K_{NI}^0 K_{IU}^0 \exp\left[\frac{(m_{NI}+m_{IU})[GuHCl]}{RT}\right]\right\} / \left\{1 + K_{NI}^0 \exp\left(\frac{m_{NI}[GuHCl]}{RT}\right) + K_{NI}^0 K_{IU}^0 \exp\left[\frac{(m_{NI}+m_{IU})[GuHCl]}{RT}\right]\right\} \quad (3)$$

The m_{NI} and m_{IU} values for the N-to-I and I-to-U transitions were fixed to 2.35 and 1.36 kcal mol^{-1} M^{-1}, respectively (*11*, *16*), assuming that the single-point mutations do not significantly affect the change in hydrophobic exposure among the N, I, and U states. Therefore, only the unfolding parameters, K_{NI}^0 and K_{IU}^0, were allowed to modulate the N-to-I and I-to-U transitions of the apo variants. The signal intensities of the N, I, and U states were either fit for each variant or fixed to WT values when poorly defined, i.e., for T67P and V68T apoMb where the N state is not completely populated after heme removal.

Fitting of HoloMb Equilibrium Unfolding Data. The equilibrium unfolding curves for the ferric holoMb variants were also obtained at single wavelengths and analyzed in terms of the six-state mechanism, which is shown in Scheme 1. This mechanism is based on the assumption that heme can bind to all three apo states. The amount of helical content was analyzed using ellipticity at 222 nm. For fluorescence detection, large emission increases were observed at 355 nm and reflect the loss of hemin, which, when bound, quenches almost all Trp fluorescence. For absorbance detection, the unfolding data were analyzed at the Soret wavelength maximum of the ferric state for each variant: 409 nm for WT, T67P, V68T, and H97D and 393 nm for H64F metMb.

The six-state unfolding model was applied to the holoMb unfolding curves. In this equilibrium model, the K_{NI}^0 and K_{IU}^0 stability constants and m_{NI} and m_{IU} values for the N-to-I and I-to-U transitions of apoMb, respectively, were determined independently in separate experiments with the apo forms and not allowed to vary. The heme dissociation constants from all possible heme-bound states, NH (metMb), IH, and UH, were allowed to vary to define the equilibrium unfolding curves for

holoMb. The three hemin dissociation constants are defined as

$$K_{NH} = \frac{[N][H]}{[NH]} = {K_{NH}}^0 \exp\left(\frac{m_{NH}[GuHCl]}{RT}\right) \quad (4)$$

$$K_{IH} = \frac{[I][H]}{[IH]} = {K_{IH}}^0 \exp\left(\frac{m_{IH}[GuHCl]}{RT}\right) \quad (5)$$

$$K_{UH} = \frac{[U][H]}{[UH]} = {K_{UH}}^0 \exp\left(\frac{m_{UH}[GuHCl]}{RT}\right) \quad (6)$$

The dependencies on GuHCl concentration are represented by m_{NH}, m_{IH}, and m_{UH}. To the best of our knowledge, m values for the dissociation of hemin from globins have never been reported, and our determination of these parameters is discussed in Results.

The population fractions of each species were computed by first obtaining the free concentration of heme [H] from the following root of a complex quadratic equation:

$$[H] = \{-(K_{NH} + K_{NH}K_{NI} + K_{NH}K_{NI}K_{IU}) + \left[(K_{NH} + K_{NH}K_{NI} + K_{NH}K_{NI}K_{IU})^2 + 4P_0\left(1 + \frac{K_{NH}K_{NI}}{K_{IH}} + \frac{K_{NH}K_{NI}K_{IU}}{K_{UH}}\right)(K_{NH} + K_{NH}K_{NI} + K_{NH}K_{NI}K_{IU})\right]^{1/2}\}/\left[2\left(1 + \frac{K_{NH}K_{NI}}{K_{IH}} + \frac{K_{NH}K_{NI}K_{IU}}{K_{UH}}\right)\right] \quad (7)$$

The fraction of each species was calculated using the free heme concentration [H], the two apoMb stability constants, and the three equilibrium constants for the dissociation of heme:

$$Y_{NH} = 1/\left(1 + \frac{K_{NH}}{[H]} + \frac{K_{NH}K_{NI}}{[H]} + \frac{K_{NH}K_{NI}K_{IU}}{[H]} + \frac{K_{NH}K_{NI}}{K_{IH}} + \frac{K_{NH}K_{NI}K_{IU}}{K_{UH}}\right) \quad (8)$$

$$Y_{IH} = \frac{K_{NH}K_{NI}}{K_{IH}}/\left(1 + \frac{K_{NH}}{[H]} + \frac{K_{NH}K_{NI}}{[H]} + \frac{K_{NH}K_{NI}K_{IU}}{[H]} + \frac{K_{NH}K_{NI}}{K_{IH}} + \frac{K_{NH}K_{NI}K_{IU}}{K_{UH}}\right) \quad (9)$$

$$Y_{UH} = \frac{K_{NH}K_{NI}K_{IU}}{K_{UH}}/\left(1 + \frac{K_{NH}}{[H]} + \frac{K_{NH}K_{NI}}{[H]} + \frac{K_{NH}K_{NI}K_{IU}}{[H]} + \frac{K_{NH}K_{NI}}{K_{IH}} + \frac{K_{NH}K_{NI}K_{IU}}{K_{UH}}\right) \quad (10)$$

$$Y_N = \frac{K_{NH}}{[H]}/\left(1 + \frac{K_{NH}}{[H]} + \frac{K_{NH}K_{NI}}{[H]} + \frac{K_{NH}K_{NI}K_{IU}}{[H]} + \frac{K_{NH}K_{NI}}{K_{IH}} + \frac{K_{NH}K_{NI}K_{IU}}{K_{UH}}\right) \quad (11)$$

$$Y_I = \frac{K_{NH}K_{NI}}{[H]}/\left(1 + \frac{K_{NH}}{[H]} + \frac{K_{NH}K_{NI}}{[H]} + \frac{K_{NH}K_{NI}K_{IU}}{[H]} + \frac{K_{NH}K_{NI}}{K_{IH}} + \frac{K_{NH}K_{NI}K_{IU}}{K_{UH}}\right) \quad (12)$$

$$Y_U = \frac{K_{NH}K_{NI}K_{IU}}{[H]}/\left(1 + \frac{K_{NH}}{[H]} + \frac{K_{NH}K_{NI}}{[H]} + \frac{K_{NH}K_{NI}K_{IU}}{[H]} + \frac{K_{NH}K_{NI}}{K_{IH}} + \frac{K_{NH}K_{NI}K_{IU}}{K_{UH}}\right) \quad (13)$$

The fraction of free hemin (Y_H) is given by the sum of the fractions of apoglobin states ($Y_N + Y_I + Y_U$). Each of the stability and affinity constants depicted in eqs 8−13 was computed at different GuHCl concentrations using the m_{NI}, m_{IU}, m_{NH}, m_{IH}, and m_{UH} values as defined in eqs 1, 2, and 4−6, respectively, to determine the fractions of each species as a function of GuHCl concentration.

The Soret absorbance, CD, and fluorescence signals were computed from

$$S = S_N Y_N + S_{NH} Y_{NH} + S_I Y_I + S_{IH} Y_{IH} + S_U Y_U + S_{UH} Y_{UH} + S_H Y_H \quad (14)$$

The fitted signal parameters (S_N through S_{UH}) for the UV−visible absorbance, CD, and fluorescence of the various unfolding states of the Mb variants are given in the Supporting Information for each of the fits shown in Figures 2 and 3, along with detailed interpretations of the differences between the states and mutants. Roughly, the normalized CD_{222} signal for all of the NH states was 1.0. The S_N(CD) values ranged from 0.7 (H64F) to 0.4 (T67P). S_I(CD) and S_{IH}(CD) were both between 0.17 and 0.55. S_U(CD) and S_{UH}(CD) were defined as ~0.0 for all the proteins. The Soret absorbance change signal for holo-metMb in the NH state, S_{NH}(Abs), was defined as 1.0 for all the variants. The S_{IH}(Abs) signal was allowed to vary. The S_{UH}(Abs) signal was set to be small. The S(Abs) values for the apoprotein species were defined as 0.0. The fluorescence change signals were defined on the basis of a normalized S_U(F) value of 1.0 for the unfolded apoMb state. S_{NH}(F) was assigned an initial value of 0.0. S_N(F) and S_I(F) were calculated using the apoMb results. S_{IH}(F) was allowed to vary. In the holoMb experiments, fluorescence was measured at 355 nm, and as a result, the signal coefficients for the N and I states obtained for the apoMb unfolding experiments do not apply directly to the holoMb experiments (see the Supporting Information).

In general, holoMb unfolding should depend on the total protein concentration because it involves dissociation of heme, which should be facilitated at low concentrations. Hargrove and Olson (*22*) examined the dependence of holoMb unfolding on total protein concentration and observed very little change in the unfolding curves over the range from 6 to 160 μM. They attributed this lack of dependence to nonspecific hemin binding to unfolded Mb. We have verified their calculations and also examined theoretically the effect of hemin dimerization following dissociation from the protein (*37*). The addition of a free hemin dimerization step after unfolding greatly complicates the analysis, leading to a cubic equation for the concentration of free monomeric hemin. We are examining this problem experimentally, which requires measuring holoMb unfolding curves over a very wide range of total protein concentrations (from 1 to 100 μM) and determining independently the dependence of hemin dimerization on GuHCl concentration. Our current results indicate that the only significant effects of including the hemin dimerization step are 2−4-fold decreases in the fitted hemin dissociation constants for the N and I states. The basic conclusions shown in Tables 1 and 2 and Figures 3−5 remain unchanged upon comparison of the Mb variants, and the structural interpretation of the IH intermediate is unaffected. Thus, for this paper, we neglected the added complexities of hemin dimerization and variation of protein concentration.

RESULTS

Equilibrium Unfolding of ApoMb Variants. The GuHCl-induced unfolding of each apo variant was monitored by far-UV circular dichroism (CD) and tryptophan fluorescence emission.

Overlays of both measurements for all variants are shown in Figure 2. In most cases, the CD data reveal an inflection point in the unfolding curves indicative of a populated intermediate; however, the CD data alone are not sufficient to define accurately the stability parameters for the N-to-I and I-to-U transitions. The fluorescence unfolding curves demonstrate unequivocally the presence of an intermediate, which is characterized by hyperfluorescence centered at a wavelength between the fluorescence peaks for the native N and unfolded U states, as observed previously (*12*, *15*, *16*). We have assumed that the signals from both CD and fluorescence emission report on the same intermediate, and as described by Hargrove et al. (*12*), Scott et al. (*16*), and Smith (*11*), the unfolding data were fit simultaneously to a three-state N-to-I-to-U equilibrium unfolding mechanism analogous to the one originally developed by Barrick, Baldwin, and colleagues (*50*−*53*). For each mutant and WT apoMb, we successfully obtained fitted K_{NI}^0 and K_{IU}^0 stability constants for the N-to-I and I-to-U transitions in the absence of denaturant, and the values are listed along with free energy parameters in Table 1.

As expected, the unfolding data for the five apoMb variants were readily interpreted in terms of a three-state model. The shape of the unfolding curve is directly influenced by the population fraction and respective signals for each of the three states, as depicted in eq 3. The populations of each state are markedly dependent on the stability constants K_{NI}^0 and K_{IU}^0, which vary between the mutants, whereas the *m* values for the two transitions are relatively invariant and were kept constant. The respective signals for the folded (N) and intermediate (I) states of each apoprotein vary due to the structural changes induced by the point mutation. These effects are most noticeable for the hyperfluorescence intensity of the molten globule intermediate in H64F, which is significantly less intense than that in H97D. This decrease in intermediate fluorescence for H64F could reflect a more compact molten globule because of its increased core hydrophobicity and stability. The CD unfolding curves also reveal a disparity between the higher helical content of the N and I states of H64F when compared to lower helical content for the same T67P states (see Table S1 of the Supporting Information).

The variants show a wide range of stabilities for the N states, with the H64F mutant being the most stable and the T67P variant being the least stable. As expected, K_{IU}^0 is much less affected by these distal pocket mutations than K_{NI}^0, supporting the view that the heme pocket is melted in the molten globule intermediate I state. The H64F substitution increases the hydrophobicity of the heme pocket, inhibiting its unfolding and decreasing K_{NI}^0 3-fold (Table 1). The H97D variant displays stabilities for the N and I states that are similar to those of WT apoMb because the imidazole side chain of residue 97 is solvent-exposed. The V68T substitution increases the polarity of the heme pocket by inserting an additional polar side chain adjacent to the ligand binding site and causes a marked decrease in the stability of the N state, which is reflected by the 6-fold increase in K_{NI}^0 (*12*). Finally, the T67P variant introduces a "kink" in the E helix, lowering its stability and that of the entire heme pocket in the N state, resulting in a dramatic 30-fold increase in K_{NI}^0.

Unfolding of WT HoloMb. The general scheme for the unfolding of a monomeric heme protein is shown in Scheme 1 and allows heme, H, to bind to all three apoprotein states (N, I, and U). The unfolding equations derived from this mechanism are given in Materials and Methods. In our analysis, the parameters for the unfolding of the apoprotein species were fixed on the basis of independent analysis of the apoglobin data shown in Figure 2. We were able to fit simultaneously the absorbance, far-UV CD, and tryptophan fluorescence unfolding curves for holoMb to the general six-state unfolding model and obtain estimates of the hemin dissociation constants [K_{NH}^0, K_{IH}^0, and K_{UH}^0 (dissociation constants in the absence of denaturant)] for the three holoMb states (Table 2).

The agreement between the observed data and the fitted curves is remarkably good (Figure 3), considering that the key apoMb unfolding parameters were fixed to the values listed in Table 1. The fractions of each state during unfolding are also shown in Figure 3. The complete set of data for all five variants demonstrates unequivocally that unfolding of holoMb is not a one-step process and involves equilibrium populations of IH and I states at moderate denaturant concentrations. However, as observed previously, the curves for WT holoMb by themselves are not definitive with respect to the presence of an IH state.

The dissociation constant K_{NH}^0 for WT holoMb was estimated to be $\sim 0.9 \times 10^{-13}$ M at pH 7 and 20 °C, which is in reasonable agreement with the equilibrium dissociation constant ($K_{-H} \sim 0.3 \times 10^{-13}$ M) computed from the ratio of dissociation and association rate constants for WT metMb at pH 7, but at a higher salt concentration in 0.45 M sucrose at 37 °C (Table 2) (*22*, *30*). In addition, we were able to successfully estimate K_{IH}^0, which is $\sim 1.4 \times 10^{-11}$ M, indicating that the hemin affinity of the WT I state is ~100-fold weaker than that of the N state. The value of K_{UH}^0 is poorly defined but estimated to be $\sim 10^{-6}$ M for all five variants, in agreement with previous estimates of heme binding to unfolding apoMb and apocytochrome b_{562} (see Discussion and refs *22* and *40*).

H64F, a Variant with Increased ApoMb Stability but Decreased Hemin Affinity. The unfolding of the H64F mutant is depicted in Figure 3. This mutant was selected because the Phe substitution increases the stability of the N state of the apo form by replacing the polar imidazole side chain with a relatively apolar aromatic ring which excludes water from the heme pocket (*5*, *12*). However, removal of the distal histidine eliminates the His64 hydrogen bond to the water molecule that is coordinated to the hemin iron atom. As a result, water is no longer bound to the iron atom, and H64F metMb is pentacoordinate, showing a much weaker Soret band at 393 nm instead of the strong 409 nm band seen for the aquomet form of WT metMb. In addition, the affinity of the N state of H64F apoMb for hemin is ~4-fold weaker than that of WT apoMb. In terms of dissociation equilibrium constants, K_{NH}(H64F) is $\sim 4 \times 10^{-13}$ M compared to K_{NH}(WT) which is $\sim 0.9 \times 10^{-13}$ M.

As observed for WT holoMb, the unfolding curves for H64F holoMb do not have obvious inflection points; however, the unfolding curves are clearly broadened, and the transition midpoints occur at a slightly higher GuHCl concentration than

Table 1: Stability Parameters for the ApoMb Variants[a]

apoMb	K_{NI}^0	K_{IU}^0	$1/K_{NU}^0$
WT	0.021	0.019	2500
H64F	0.0061	0.011	15000
T67P	0.67	0.029	51
V68T	0.13	0.017	450
H97D	0.013	0.061	1300

[a]The GuHCl-induced unfolding measurements were taken in 10 mM potassium phosphate at pH 7 and 20 °C. K_{NI}^0 and K_{IU}^0 were obtained by fitting simultaneously both CD and fluorescence signals for the unfolding of the apoMb variants to the three-state unfolding mechanism using eq 3 (see Table S1 of the Supporting Information). The values of m_{NI} and m_{IU} were set to 2.35 and 1.36 kcal mol^{-1} M^{-1}, respectively.

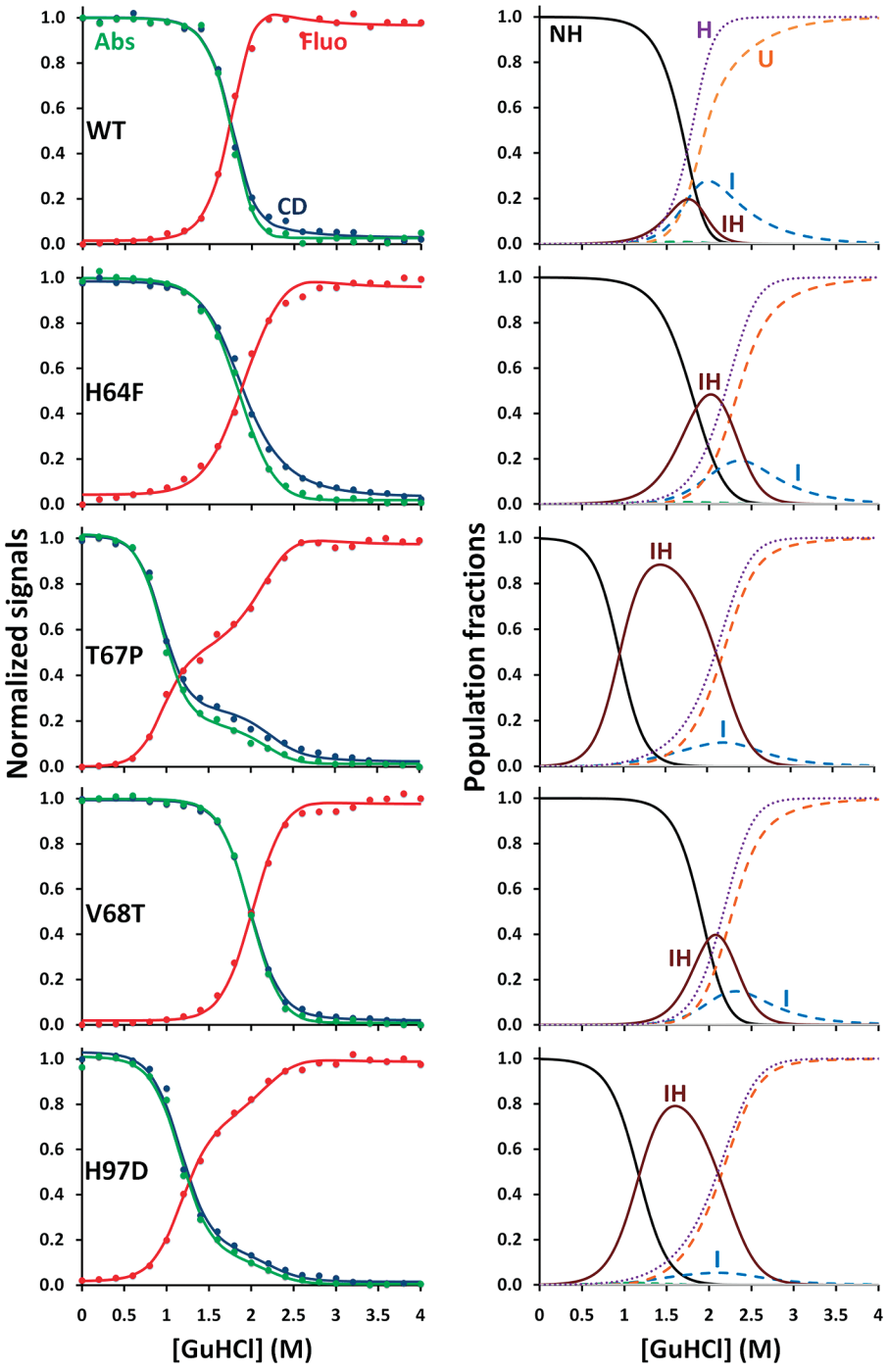

FIGURE 3: GuHCl-induced equilibrium unfolding of holoMb variants. The left panels represent the unfolding data from far-UV CD at 222 nm (blue), fluorescence emission at 355 nm (red), and Soret absorbance (green), with the best fit to the six-state unfolding model. The right panels depict the population fractions of each species with regard to GuHCl concentration. Conditions: 10 μM protein, 10 mM potassium phosphate, pH 7, 20 °C.

Table 2: Hemin Dissociation Constants and *m* Values for the NH and IH States of Holo-metMb Variants[a]

holoMb	K_{NH}^0 (M)	m_{NH} (kcal mol^{-1} M^{-1})	K_{IH}^0 (M)	m_{IH} (kcal mol^{-1} M^{-1})	K_{-H} (M) at pH 7−8[b]	K_{-H} (M) at pH 5[b]
WT	0.88×10^{-13}	4.4	1.4×10^{-11}	4.0	0.28×10^{-13}	28×10^{-13}
H64F	4.1×10^{-13}	3.5	1.0×10^{-11}	3.3	2.2×10^{-13}	130×10^{-13}
T67P	1.0×10^{-13}	4.3	3.6×10^{-11}	2.8	not determined	not determined
V68T	0.016×10^{-13}	4.1	1.5×10^{-11}	3.2	$\leq 0.05 \times 10^{-13}$	1.1×10^{-13}
H97D	84×10^{-13}	3.4	8.8×10^{-11}	2.4	180×10^{-13}	1100×10^{-13}

[a]The unfolding measurements were taken in 0.01 M potassium phosphate at pH 7 and 20 °C. K_{UH}^0 and m_{UH} were fixed to 1.0 x10^{-6} M and 2.4 kcal mol^{-1} M^{-1}, respectively, for all five variants as described in Discussion. The CD, fluorescence, and Soret absorbance signal parameters are given in Table S2 of the Supporting Information. [b]The values for K_{-H} were computed from the hemin dissociation rate constants assuming that the association rate constant is 1.0×10^8 M^{-1} s^{-1} for all five variants, as described by Hargrove et al. (*30*). The dissociation rate constants were taken from data at pH 7 and 5 at 37 °C in 0.45 M sucrose and 0.15 M sodium phosphate or acetate, respectively (*22*, *29*). Unfortunately, the dissociation rate constant for H64F at pH 7 reported by Hargrove et al. (*29*) is a misprint (i.e., the real value is 0.1 h^{-1} and not 0.01 h^{-1}). We used the value of 0.08 h^{-1}, which was measured by Hargrove et al. (*39*).

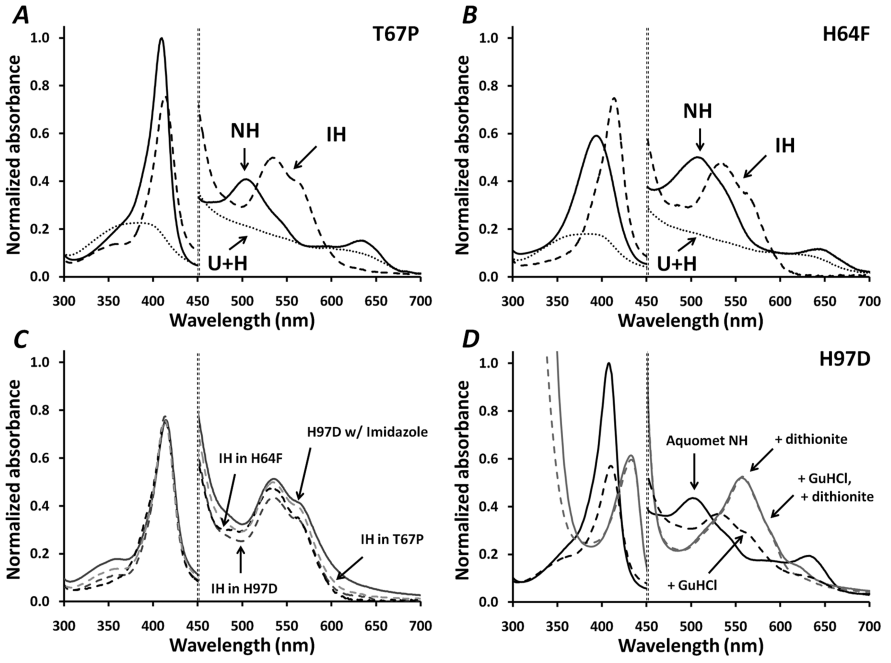

FIGURE 4: (A and B) Absorbance spectra of T67P and H64F in the native folded NH, IH, and U + H states. All absorbance values were normalized to the peak absorbance of WT metMb at 409 nm at 10 μM total heme, which was the concentration used for all the samples. The normalized scale for the visible region (450−700 nm) is 0−0.15. Deconvoluted spectra for the IH states were computed assuming the starting NH and final U + H states shown in the panels and then subtracting weighted sums of these spectra from the spectra measured at the midpoint GuHCl concentration where the fraction of the IH state is the largest. The fractions of NH, IH, and free H at the intermediate GuHCl concentration were estimated from the fitted parameters in Table 2 and eqs 8−13. (C) Overlay of the deconvoluted spectra of the IH states for T67P, H64F, and H97D Mb obtained from the GuHCl titrations and the spectrum of imidazole bound to H97D metMb (at 100 mM free imidazole). (D) Spectra for H97D holo-metMb in the absence (solid line) and presence (dashed line) of 1.4 M GuHCl, before reduction (black) and after addition of sodium dithionite (gray). Buffer conditions: 10 mM potassium phosphate, pH 7, 20 °C.

those for WT holoMb. Fitting to the six-state model suggests the presence of a significant population of the IH state during unfolding, which causes broadening of the overall unfolding transition. Fitting to a two-state model would require a significant decrease in the overall unfolding *m* value, which is unlikely to be caused by a single point mutation. The lower value of K_{NH}^0 for H64F metMb is in agreement with the smaller value estimated from the ratio of the dissociation and association rate constants for hemin binding to this mutant (Table 2) (*29*). The equilibrium constant for dissociation of hemin from the mutant IH state, K_{IH}^0, is estimated to be 1.0×10^{-11} M, which is similar to that for the WT Mb intermediate (Table 2).

The presence of an IH state during unfolding of H64F holoMb is suggested by a red shift of the Soret band to 410 nm at a GuHCl concentration favoring ~50% net unfolding. We deconvoluted the UV−visible absorbance spectra of H64F holoMb/GuHCl mixtures near the unfolding midpoint to obtain the absolute spectrum of the IH state. The result is shown in Figure 4B. Interestingly, the deconvoluted IH spectrum is characteristic of a hemichrome species with a Soret maximum at 415 nm, a major low-spin β band at 535 nm, and an α band shoulder at 565 nm (*35*). Thus, we propose that the IH state in Mb is a hemichrome. Unfolding of the heme pocket of the holoprotein appears to allow formation of a bis-histidyl linkage to the heme iron even in the absence of a distal histidine. Thus, the hemichrome-like IH state may involve bis-His coordination by alternative sets of two histidines in the heme pocket region, and not just His64 and His93 (Figure 1). Alternatively, the bis-axial coordination could arise from a Met/His pair, and there is one Met side chain in the heme pocket region, Met55(D5).

T67P: A Variant with Wild-Type Hemin Affinity but an Unstable N State. The unfolding of the holo T67P mutant is depicted in Figure 3. This mutant was selected as a variant with a highly destabilized apoglobin N state (Table 1, largest K_{NI}^0 value) due to insertion of proline in the middle of the E helix (Figure 1). However, the affinity of the apoprotein N state for hemin is similar to that of WT Mb. The unfolding curves of T67P holoMb all show well-defined inflection points, which demonstrate unambiguously the presence of an intermediate species. These data were readily fit to the six-state model, and the major intermediate species is the IH state, which dominates at ~1.4 M GuHCl. The IH state for this mutant is favored because of the instability of the apoMb N state, which facilitates partial unfolding even with the hemin cofactor bound. Analysis of the UV−visible absorbance spectra during unfolding reveals directly that the IH state is a hemichrome-like species, which is characterized by distinct absorbance bands at 415, 535, and 565 nm (*35*). For this mutant, the hemichrome spectrum can be observed almost by itself at the midpoint GuHCl concentration because the fraction of IH is ~0.90 (Figure 3). The deconvoluted spectrum of the IH state for T67P metMb is shown in panels A and C of Figure 4.

The fitted parameters for T67P metMb unfolding are listed in Tables 1 and 2. As expected, this mutation does not affect heme affinities, and the computed hemin dissociation constants remain similar to those for WT metMb with a K_{NH}^0 of ~1.0×10^{-13} M and a K_{IH}^0 of ~3.6×10^{-11} M (Table 2). Only the apoMb N-to-I unfolding parameters are affected by the T67P substitution (Table 1). However, the large increase in K_{NI}^0 causes a marked effect on the holoMb unfolding curves and a dramatic increase in the population of the IH state, allowing its spectral properties to be characterized and assigned unambiguously to a hemichrome species.

V68T: A Variant with Increased Heme Affinity but Decreased Stability of the N State. The V68T mutant was

selected as a variant with an unstable N apoMb state (i.e., increased K_{NI}^0) but a markedly increased affinity for heme (*22*). The Thr68 hydroxyl group forms an additional strong hydrogen bond with coordinated water, which stabilizes bound hemin, reduces its rate of dissociation, and decreases K_{NH}^0 markedly (*22*).

As observed for WT metMb, the unfolding curves for V68T holoMb appear to be highly cooperative and indicative of a two-state mechanism, but the holoprotein unfolding transition is shifted toward a higher GuHCl concentration, i.e., ~2.0 M (Figure 3). Fitting of these data to the six-state unfolding model reveals that the increase in the transition midpoint is caused by an ~50-fold increase in the heme affinity of the N state (K_{NH}^0 decreases from ~0.9 to ~0.02×10^{-13} M) even though the stability of the N apoprotein state is decreased ~5-fold [K_{NI}^0 increases from 0.02 to 0.13 (Table 1)]. The fits do suggest the presence of an IH state during unfolding, but it is present at ≤40% at the unfolding midpoint. We were able to deconvolute a hemichrome spectrum at this denaturant concentration, but the noise was considerable due to the smaller population of IH and larger amounts of NH and U + H states. As is the case for the other mutants, the fitted parameters suggest that the affinity of the I state for hemin is similar to that for the WT intermediate with a K_{IH}^0 of ~1.7×10^{-11} M (Table 2).

H97D Mb: A Variant with a Markedly Decreased Heme Affinity but Wild-Type ApoMb Stability. The H97D mutant has an ~100-fold decreased affinity for hemin while retaining N and I apo state stabilities similar to those for WT Mb. The H97D substitution disrupts favorable electrostatic interactions among the His97 side chain, the Ser92 hydroxyl group on the F helix, and the heme 7-propionate (*54*). This disruption markedly increases the rate of hemin dissociation and the equilibrium dissociation constant (K_{NH}^0) but has little or no effect on the unfolding of apoMb (Figure 2, Table 1, and ref *22*).

The unfolding curves for H97D metMb (Figure 3) all show inflection points, demonstrating unambiguously the presence of an intermediate, and the fitted parameters show that the biphasic nature of the curves is caused by population of the IH state, which reaches a maximum of ~80% at ~1.5 M GuHCl. As is the case for the T67P mutant, the absorbance spectrum of H97D metMb at ~1.5 M GuHCl indicates a hemichrome species (Figure 4D). The deconvoluted spectrum for the IH state of H97D Mb is shown in Figure 4C and is identical to that of the IH species for T67P and H64F Mb.

The fitted parameters for H97D holoMb show that the N state has an ~100-fold lower affinity for hemin, with a K_{NH}^0 of 84×10^{-13} M, which is similar to that estimated previously from association and dissociation rate constants for hemin binding to this mutant (Table 2) (*22*). The affinity of the I state of H97D Mb for hemin is also lower, with a K_{IH}^0 increasing from ~1.4 to ~8.8×10^{-11} M. This ~6-fold decrease in affinity suggests that the unfavorable electrostatic interactions caused by the H97D mutation at the FG loop also weaken the affinity of the I state for hemin even though the heme pocket is unfolded.

The IH State Is a Hemichrome. All the Mb variants appear to populate an IH state during unfolding of the holoprotein, but the extent varies greatly from ≤20% for WT holoMb to ~80 and ~90% for the H97D and T67P mutants, respectively. The deconvoluted absolute spectra of the IH state for the T67P and H64F variants are shown in Figures 4A and 4B, respectively, and compared to the starting spectra of metMb and that of the final U state with free hemin. The deconvoluted IH spectra of the three variants showing the highest population of IH states are overlaid in Figure 4C and compared to that for H97D metMb titrated with excess imidazole (100 mM, pH 7) to create a bis-imidazole hemichrome in the NH state. All four spectra are superimposable and display the low-spin peak at 535 nm, the 565 nm shoulder, and the red-shifted Soret band at 415 nm, characteristic of a bis-histidyl or a methionyl-histidyl hemichrome.

Surprisingly, the IH species appears to exhibit ~40% of the fluorescence of the completely unfolded U state even though hemin is still bound. This property is clear for T67P Mb (Figure 3). At 1.4 M GuHCl, IH is the dominant species with a clear hemichrome UV−visible spectrum, roughly the same CD signal as the I state of T67P apoMb (~30% of completely folded holoMb), and roughly 40% of the fluorescence of the U state of apoMb. Because hemin is still bound, we expected that the Trp fluorescence would remain almost completely quenched, but it is not. This result suggests that the angle for fluorescence resonance energy transfer is much less favorable than in the native state, expansion of the heme pocket size has moved the porphyrin ring farther from the two Trp side chains positioned along the A helix, and/or the enhanced mobility of the Trp residues in this molten globule state reduces the level of both solvent quenching and resonance energy transfer.

The hemichromes involved in Hb and Mb degradation have often been associated with irreversibility (*35*). However, the GuHCl-induced unfolding curves for holo-metMb are reversible and independent of how the mixtures are made. We conducted kinetic experiments in which holoMb at a high GuHCl concentration was rapidly diluted into buffer and vice versa. The same equilibrium state was obtained in each case. For example, upon dilution into buffer, the hemichrome IH state of H97D induced by 1.4 M GuHCl refolds, within the dead time of our stopped-flow apparatus, into the native metMb form with a "normal" Soret maximum at 409 nm and visible absorbance bands at 505 and 630 nm indicative of high-spin aquohemin.

We also tested whether the IH hemichrome in H97D could refold into a native-like pentacoordinate deoxyMb state after rapid reduction. As shown in Figure 4D, when H97D metMb in 1.4 M GuHCl is reduced anaerobically with a slight excess of sodium dithionite, a normal, pentacoordinate deoxyMb species was formed immediately and showed a broad Soret maximum at 434 nm and a single visible absorbance band centered at 558 nm. No evidence of a hemochrome (bis-imidazole complex with heme iron in the reduced state) spectrum was observed under these conditions at 1.4 M GuHCl, which Hargrove and Olson (*22*) showed is too small to induce any denaturation of WT or H97D deoxyMb. Wittung-Stafshede et al. (*55*) conducted a similar experiment with native metMb denatured with 2.5 M GuHCl. In their experiment, reduction was induced by photoexcitation of NADH with a nanosecond Nd:YAG laser. Almost completely denatured metMb folded into pentacoordinate, native-like deoxyMb within 2−3 ms ($\tau \approx 0.3$ ms) after photoreduction. Thus, the hemichrome IH intermediate appears to be fully reversible and able to fold back rapidly into highly stable ferric or reduced NH states.

m Values for Hemin Dissociation Constants. In our analysis, we have assumed that all three hemin dissociation constants are increased in the presence of GuHCl and that there is a linear free energy relationship between $\Delta G°$ for hemin dissociation and GuHCl concentration, as expressed by eqs 4−6. If K_{NH} were independent of GuHCl concentration, and the denaturant affected only the apoMb unfolding constants as shown in Figure 2, then the computed $[GuHCl]_{1/2}$ would be ~3.5 M for WT holoMb, which is markedly greater than the observed value

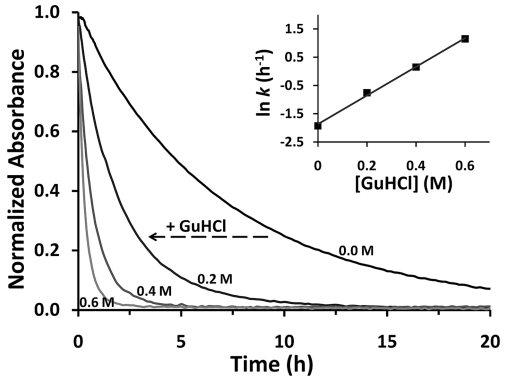

FIGURE 5: Kinetic traces for loss of hemin from H97D aquomet Mb as a function of GuHCl concentration. The four traces represent normalized absorbance change time courses at 409 nm as a function of GuHCl concentration, which is listed beside each curve. In these experiments, 4 μM H97D aquometMb was mixed with 40 μM H64Y/V68F apoMb, which acts as a hemin scavenging agent (*38*), in 10 mM potassium phosphate at pH 7 and 20 °C. For the inset, the observed hemin dissociation rate constants were obtained from fits to a single-exponential process for each trace. A plot of the natural logarithm of these rates vs GuHCl concentration is shown in the inset.

of ~1.8 M (Figure 3). Thus, it is clear that GuHCl induces hemin dissociation, and the fitted m_{NH}, m_{IH}, and m_{UH} values help define the steepness and transition midpoint of the holoMb unfolding curves. The absolute values of m_{NH} and m_{IH} are unexpectedly larger than those for the N-to-I and I-to-U transitions of apoMb, 4.4−2.4 kcal mol^{-1} M^{-1} for hemin dissociation versus 2.3−1.4 kcal mol^{-1} M^{-1} for apoglobin unfolding.

To verify the strong dependence of K_{NH} on GuHCl concentration, we measured the rate of hemin loss from H97D metMb as a function of GuHCl concentration in the range from 0.0 to 0.6 M, and the results are shown in Figure 5. These experiments were conducted under the conditions used for equilibrium unfolding (10 mM phosphate, pH 7, 20 °C) and in the absence of sucrose, which is normally added as a stabilizing agent to inhibit precipitation of the resulting apoglobin (*39*). As a result, the observed rate of dissociation of hemin from H97D metMb is much slower than that reported previously for this mutant in high salt and sucrose at 37 °C (*29*). As predicted from the results in Table 2, the rate of hemin dissociation depends strongly on GuHCl concentration, even at these low concentrations where little or no net equilibrium unfolding occurs (see 0 to 0.6 M GuHCl regions in Figure 3). The observed rate of loss of hemin from H97D metMb increases from ~0.15 h^{-1} at 0 M to ~4 h^{-1} at 0.6 M GuHCl. A plot of ln $k_{-\text{hemin}}$ versus GuHCl concentration is linear with an apparent m value for the kinetic free energy barrier to hemin dissociation of ~3.0 kcal mol^{-1} M^{-1}. This value is large and on the order of those obtained for equilibrium hemin dissociation from the NH and IH states of this mutant [i.e., $m_{NH} \sim 4$, and $m_{IH} \sim 3$ kcal mol^{-1} M^{-1} (Table 2)]. The agreement between the kinetic and equilibrium m values for hemin dissociation appears reasonable considering the difference in the type of free energy measurement, i.e., equilibrium $\Delta G°$ versus kinetic $\Delta G^{‡}$ determinations.

DISCUSSION

Relevance of ApoMb Unfolding to the Assembly and Denaturation of the Holoprotein. The unfolding of apoMb has been studied in great detail over the past 20 years. The three-state mechanism is well-established, and the structural nature of the molten globule intermediate or I state has been characterized by both mutagenesis and NMR approaches (*14*, *17*, *19*, *56*). However, the relevance and applicability of these results to understanding both the assembly and denaturation of holoMb had not been established and were the goals of this work. The key problem is that chemical or thermal unfolding of WT holoMb is highly concerted and superficially resembles a two-state process because of the high affinity of the N apoMb state for hemin (Figure 3, top panels). In this case, the concentration of denaturant required to dissociate hemin from the N state is higher than that required to unfold the initial apoprotein N state and the partially unfolded molten globule I state. To resolve the role of the apoglobin intermediate in holoprotein unfolding and assembly, we expanded our previous work (*22*) to include a combined analysis of the unfolding of WT and four holoMb mutants. The mutations were designed to vary the stability of the apoMb N state and its affinity for heme to visualize heme binding to the apoglobin folding intermediate. As shown in Figure 3, this mutagenesis approach was successful. Our underlying assumption is that the same basic six-state mechanism applies to all five variants and that the mutations affect only the hemin dissociation and apoglobin unfolding parameters. The success of the fits and correlations of the parameter changes with expected structural effects imply that this assumption is a good approximation. Thus, one key conclusion is that the well-established mechanism for apoMb unfolding is directly relevant to holoMb unfolding and assembly, particularly when interpreting the effects of mutagenesis on overall stability and the appearance of intermediates.

These results are also relevant to holoprotein assembly in vivo. Graves et al. (*31*) and others (*11*, *12*, *16*) have suggested that expression levels of hologlobins in bacteria are proportional to the stabilities of the corresponding apoproteins because heme insertion is often limiting when high-copy number plasmids are used and maximal transcription is induced. Under these conditions, the rate of holoprotein production is determined by the rate of heme synthesis or transport times the fraction of apoglobin that is folded and competent to bind heme (*31*). One key question in this interpretation is whether heme can bind to the molten globule apoglobin intermediate and facilitate formation of the holoprotein.

IH Hemichrome and HoloMb Assembly. Hemichromes have long been associated with irreversible degradation of Hb and formation of Heinz bodies in red cells (*35*), and presumably similar degradation processes occur for Mb in vitro or in myocytes. Our results in Figures 3 and 4 show that sperm whale Mb unfolds via an IH state, which displays the spectrum of a hemichrome with a bis-histidyl linkage. The observation of a hemichrome spectrum for the H64F variant demonstrates that the distal histidine is not needed to produce the low-spin IH complex. Thus, the hemichrome spectrum is probably due a mixture of bis-imidazole or methionyl-histidyl complexes involving any two of the histidines located in the region of the heme pocket, His24(B5), His36(C1), His48(CD6), His64(E7), His81(EF loop), His82(EF loop), His93(F8), and His97(FG loop), or one of these histidines and Met55(D5). The proposed flexibility of the molten I and IH states appears to allow different combinations, although the simplest structural interpretation for most of the variants would be axial ligation by the distal and proximal histidines (His64 and His93) when they are both present.

Reversible hemichrome formation is a general phenomenon and observed during either GuHCl- or urea-induced denaturation of both sperm whale and horse heart Mb (not shown). Hemichrome formation is fully reversible, and the IH state reverts to the native metMb form with distal water coordinated to the iron atom upon rapid dilution of GuHCl. Similarly, the IH

hemichrome does not form a hemochrome when reacted with dithionite. Instead, the IH state rapidly converts to a native pentacoordinate deoxyMb form upon reduction (Figure 4D), and previous laser-induced reduction experiments suggest that this process occurs in milliseconds (*55*). Our equilibrium results suggest that hemin can bind with reasonably high affinity to the I state and promote formation of the native holoprotein. This pathway for assembly is even more probable under microaerobic conditions similar to those found in *E. coli* growing in logarithmic phase and, presumably, in respiring myocytes. Under these conditions, free heme still rapidly autoxidizes, but reduction of the ferric IH state leads to rapid formation of very stable deoxy- or oxy-holoMb states.

Hemin Binding to the N, I, and U ApoMb States. It was difficult to determine the N- and I-state hemin dissociation equilibrium constants accurately without fixing the value of the equilibrium constant for hemin dissociation from the unfolded state. K_{UH}^0 is poorly defined in our experiments at an initial holoMb concentration of 10 μM because no significant amount of UH occurs at high GuHCl concentrations (Figure 3). Separate gel filtration chromatography experiments suggest complete hemin dissociation upon unfolding of ~10 μM metMb at ≥3 M GuHCl (not shown). Spectra of the Mb variants equilibrated in 3 M GuHCl resemble that of free hemin in 3 M GuHCl. We fixed K_{UH}^0 at 1.0×10^{-6} M in our model on the basis of the affinity constants measured for nonspecific hemin binding to unfolded apocytochrome b_{562} (*40*) and native bovine serum albumin (*30*, *57*) and on the estimation that nonspecific hemin binding to unfolded apoMb is ~10^6−10^7-fold weaker than binding to the folded N apo state (*22*). Fixing K_{UH}^0 to 10^{-6} M and K_{NI}^0 and K_{IU}^0 to the values determined in separate experiments with the apoMb variants allowed determination of the equilibrium dissociation constants for hemin binding to the N and I apoglobin states.

The results in Tables 1 and 2 and the fits in Figure 3 show that distal pocket mutations affect primarily the stability of the N state and its affinity for hemin. The variations in K_{NI}^0 and K_{NH}^0 (~1000-fold) are markedly greater than those for K_{IU}^0 and K_{IH}^0 (~6-fold). These results strongly verify the interpretation of Baldwin, Barrick, Wright, and co-workers (*14*, *17*, *19*, *56*) that the N-to-I and NH-to-IH transitions involve unfolding of the heme pocket to generate a molten globule intermediate with intact A, G, and H helices.

Another key result is the fact that the variation in K_{NH}^0 values determined by analysis of holoMb unfolding curves corresponds well with equilibrium hemin dissociation constants, K_{-H}, calculated from the ratio of association and dissociation rate constants for hemin binding to the same set of Mb mutants [Table 2, last two columns (*22*, *29*, *30*)]. As shown in Figure 6, there is a strong, linear correlation between the values of $-\log(K_{NH}^0)$ obtained independently from unfolding curves and the values of $-\log(K_{-H})$ determined from kinetic experiments at both neutral and low pH. The neutral-pH values of K_{-H} are poorly defined because the rates of dissociation of hemin from WT metMb and the other higher-affinity mutants are very small and difficult to measure. At pH 5, hemin dissociation is more readily measured because of the increased level of protonation of the proximal histidine (His93) which promotes breakage of the Fe−imidazole bond (*29*). Despite the differences in solvent conditions and temperature, both the absolute values of K_{NH}^0 and the effects of mutagenesis correlate remarkably well with the K_{-H} values for WT, H64F, V68T, and H97D, determined kinetically at both pH values (Table 2 and Figure 6). Thus, GuHCl-induced unfolding curves of holo-heme proteins represent an alternative assay to measure accurately the affinities of apoproteins for hemin if the mechanism for unfolding of the apoprotein is known.

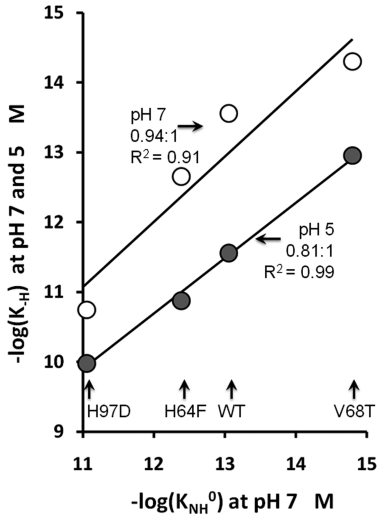

FIGURE 6: Correlations between the hemin dissociation equilibrium constant, K_{NH}^0, obtained from the analysis of the GuHCl unfolding curves shown in Figure 3 and hemin dissociation equilibrium constants, K_{-H}, calculated from the ratio of the association and dissociation rates constants measured independently in kinetic experiments (*22*, *29*, *30*). The rate parameters are listed in Table 2. The white circles represent K_{-H} values at pH 7−8 and the gray circles K_{-H} values at pH 5. The solid lines represent linear fits for $-\log(K_{NH}^0)$ vs $-\log(K_{-H})$, with the slopes and R^2 values listed beside each set of data. The K_{NH}^0 values were measured in 0.01 M potassium phosphate at pH 7 and 20 °C. Most of the K_{-H} values were obtained from measurements in either 0.15 M sodium phosphate and 0.45 M sucrose at pH 7.0 or 0.15 M acetate and 0.45 M sucrose (pH 5), each at 37 °C. The correlations are very strong, despite the differences in conditions.

ACKNOWLEDGMENT

We thank Eileen W. Singleton for assistance in expression and purification of the Mb variants.

SUPPORTING INFORMATION AVAILABLE

Signal parameters for analysis of apoMb unfolding curves using the three-state mechanism (Table S1) and signal parameters for the fitting of the holoMb variants to the six-state mechanism (Table S2). This material is available free of charge via the Internet at http://pubs.acs.org.

REFERENCES

1. Antonini, E., and Brunori, M. (1971) Hemoglobin and myoglobin in their reactions with ligands, North-Holland Publishing Co., Amsterdam.
2. Kendrew, J. C., Bodo, G., Dintzis, H. M., Parrish, R. G., Wyckoff, H., and Phillips, D. C. (1958) A three-dimensional model of the myoglobin molecule obtained by X-ray analysis. *Nature 181*, 662–666.
3. Dintzis, H. M. (1961) Assembly of the peptide chains of hemoglobin. *Proc. Natl. Acad. Sci. U.S.A. 47*, 247–261.
4. Rossi-Fanelli, A., Antonini, E., and Caputo, A. (1964) Hemoglobin and Myoglobin. *Adv. Protein Chem. 19*, 73–222.

5. Quillin, M. L., Arduini, R. M., Olson, J. S., and Phillips, G. N., Jr. (1993) High-resolution crystal structures of distal histidine mutants of sperm whale myoglobin. *J. Mol. Biol. 234*, 140–155.
6. Eliezer, D., and Wright, P. E. (1996) Is apomyoglobin a molten globule? Structural characterization by NMR. *J. Mol. Biol. 263*, 531–538.
7. Cocco, M. J., and Lecomte, J. T. (1990) Characterization of hydrophobic cores in apomyoglobin: A proton NMR spectroscopy study. *Biochemistry 29*, 11067–11072.
8. Hughson, F. M., Wright, P. E., and Baldwin, R. L. (1990) Structural characterization of a partly folded apomyoglobin intermediate. *Science 249*, 1544–1548.
9. Balestrieri, C., Colonna, G., Giovane, A., Irace, G., and Servillo, L. (1976) Equilibrium evidence of non-single step transition during guanidine unfolding of apomyoglobins. *FEBS Lett. 66*, 60–64.
10. Kirby, E. P., and Steiner, R. F. (1970) The tryptophan microenvironments in apomyoglobin. *J. Biol. Chem. 245*, 6300–6306.
11. Smith, L. (2003) The effects of amino acid substitution on apomyoglobin stability, folding intermediates, and holoprotein expression. Ph.D. Thesis, Rice University, Houston.
12. Hargrove, M. S., Krzywda, S., Wilkinson, A. J., Dou, Y., Ikeda-Saito, M., and Olson, J. S. (1994) Stability of myoglobin: A model for the folding of heme proteins. *Biochemistry 33*, 11767–11775.
13. Hughson, F. M., and Baldwin, R. L. (1989) Use of site-directed mutagenesis to destabilize native apomyoglobin relative to folding intermediates. *Biochemistry 28*, 4415–4422.
14. Barrick, D., and Baldwin, R. L. (1993) Three-state analysis of sperm whale apomyoglobin folding. *Biochemistry 32*, 3790–3796.
15. Ramsay, G., Ionescu, R., and Eftink, M. R. (1995) Modified spectrophotometer for multi-dimensional circular dichroism/fluorescence data acquisition in titration experiments: Application to the pH and guanidine-HCI induced unfolding of apomyoglobin. *Biophys. J. 69*, 701–707.
16. Scott, E. E., Paster, E. V., and Olson, J. S. (2000) The stabilities of mammalian apomyoglobins vary over a 600-fold range and can be enhanced by comparative mutagenesis. *J. Biol. Chem. 275*, 27129–27136.
17. Jennings, P. A., and Wright, P. E. (1993) Formation of a molten globule intermediate early in the kinetic folding pathway of apomyoglobin. *Science 262*, 892–896.
18. Loh, S. N., Kay, M. S., and Baldwin, R. L. (1995) Structure and stability of a second molten globule intermediate in the apomyoglobin folding pathway. *Proc. Natl. Acad. Sci. U.S.A. 92*, 5446–5450.
19. Nishimura, C., Dyson, H. J., and Wright, P. E. (2006) Identification of native and non-native structure in kinetic folding intermediates of apomyoglobin. *J. Mol. Biol. 355*, 139–156.
20. Nishimura, C., Wright, P. E., and Dyson, H. J. (2003) Role of the B helix in early folding events in apomyoglobin: Evidence from site-directed mutagenesis for native-like long range interactions. *J. Mol. Biol. 334*, 293–307.
21. Pinker, R. J., Lin, L., Rose, G. D., and Kallenbach, N. R. (1993) Effects of alanine substitutions in α-helices of sperm whale myoglobin on protein stability. *Protein Sci. 2*, 1099–1105.
22. Hargrove, M. S., and Olson, J. S. (1996) The stability of holomyoglobin is determined by heme affinity. *Biochemistry 35*, 11310–11318.
23. Moczygemba, C., Guidry, J., and Wittung-Stafshede, P. (2000) Heme orientation affects holo-myoglobin folding and unfolding kinetics. *FEBS Lett. 470*, 203–206.
24. Lin, L., Pinker, R. J., Phillips, G. N., and Kallenbach, N. R. (1994) Stabilization of myoglobin by multiple alanine substitutions in helical positions. *Protein Sci. 3*, 1430–1435.
25. Garcia-Moreno, B., Chen, L. X., March, K. L., Gurd, R. S., and Gurd, F. R. (1985) Electrostatic interactions in sperm whale myoglobin. Site specificity, roles in structural elements, and external electrostatic potential distributions. *J. Biol. Chem. 260*, 14070–14082.
26. Flanagan, M. A., Garcia-Moreno, B., Friend, S. H., Feldmann, R. J., Scouloudi, H., and Gurd, F. R. (1983) Contributions of individual amino acid residues to the structural stability of cetacean myoglobins. *Biochemistry 22*, 6027–6037.
27. Gupta, R., Yadav, S., and Ahmad, F. (1996) Protein stability: Urea-induced versus guanidine-induced unfolding of metmyoglobin. *Biochemistry 35*, 11925–11930.
28. Hargrove, M. S., Whitaker, T., Olson, J. S., Vali, R. J., and Mathews, A. J. (1997) Quaternary structure regulates hemin dissociation from human hemoglobin. *J. Biol. Chem. 272*, 17385–17389.
29. Hargrove, M. S., Wilkinson, A. J., and Olson, J. S. (1996) Structural factors governing hemin dissociation from metmyoglobin. *Biochemistry 35*, 11300–11309.
30. Hargrove, M. S., Barrick, D., and Olson, J. S. (1996) The association rate constant for heme binding to globin is independent of protein structure. *Biochemistry 35*, 11293–11299.
31. Graves, P. E., Henderson, D. P., Horstman, M. J., Solomon, B. J., and Olson, J. S. (2008) Enhancing stability and expression of recombinant human hemoglobin in *E. coli*: Progress in the development of a recombinant HBOC source. *Biochim. Biophys. Acta 1784*, 1471–1479.
32. Looker, D., Abbott-Brown, D., Cozart, P., Durfee, S., Hoffman, S., Mathews, A. J., Miller-Roehrich, J., Shoemaker, S., Trimble, S., and Fermi, G.; et al. (1992) A human recombinant haemoglobin designed for use as a blood substitute. *Nature 356*, 258–260.
33. Wagenbach, M., O'Rourke, K., Vitez, L., Wieczorek, A., Hoffman, S., Durfee, S., Tedesco, J., and Stetler, G. (1991) Synthesis of wild type and mutant human hemoglobins in *Saccharomyces cerevisiae*. *Nat. Biotechnol. 9*, 57–61.
34. Winterbourn, C. C., and Carrell, R. W. (1974) Studies of hemoglobin denaturation and Heinz body formation in the unstable hemoglobins. *J. Clin. Invest. 54*, 678–689.
35. Rifkind, J. M., Abugo, O., Levy, A., and Heim, J. (1994) Detection, formation, and relevance of hemichromes and hemochromes. *Methods Enzymol. 231*, 449–480.
36. Peisach, J., Blumberg, W. E., Wittenberg, B. A., Wittenberg, J. B., and Kampa, L. (1969) Hemoglobin A: An electron paramagnetic resonance study of the effects of interchain contacts on the heme symmetry of high-spin and low-spin derivatives of ferric α chains. *Proc. Natl. Acad. Sci. U.S.A. 63*, 934–939.
37. Culbertson, D. S., and Olson, J. S. (2010) Folding and Assembly of Myoglobins and Hemoglobins. In Protein Folding and Metal Ions: Mechanisms, Biology, and Disease (Wittung-Stafshede, P., and Gomes, C. M., Eds.) Taylor and Francis, Inc., London.
38. Gibson, Q. H., and Antonini, E. (1960) Kinetic studies on the reaction between native globin and haem derivatives. *Biochem. J. 77*, 328–341.
39. Hargrove, M. S., Singleton, E. W., Quillin, M. L., Ortiz, L. A., Phillips, G. N., Jr., Olson, J. S., and Mathews, A. J. (1994) His64(E7)→Tyr apomyoglobin as a reagent for measuring rates of hemin dissociation. *J. Biol. Chem. 269*, 4207–4214.
40. Robinson, C. R., Liu, Y., Thomson, J. A., Sturtevant, J. M., and Sligar, S. G. (1997) Energetics of heme binding to native and denatured states of cytochrome b562. *Biochemistry 36*, 16141–16146.
41. Springer, B. A., and Sligar, S. G. (1987) High-level expression of sperm whale myoglobin in *Escherichia coli*. *Proc. Natl. Acad. Sci. U.S.A. 84*, 8961–8965.
42. Carver, T. E., Brantley, R. E., Jr., Singleton, E. W., Arduini, R. M., Quillin, M. L., Phillips, G. N., Jr., and Olson, J. S. (1992) A novel site-directed mutant of myoglobin with an unusually high O_2 affinity and low autooxidation rate. *J. Biol. Chem. 267*, 14443–14450.
43. Springer, B. A., Egeberg, K. D., Sligar, S. G., Rohlfs, R. J., Mathews, A. J., and Olson, J. S. (1989) Discrimination between oxygen and carbon monoxide and inhibition of autooxidation by myoglobin. Site-directed mutagenesis of the distal histidine. *J. Biol. Chem. 264*, 3057–3060.
44. Ascoli, F., Fanelli, M. R., and Antonini, E. (1981) Preparation and properties of apohemoglobin and reconstituted hemoglobins. *Methods Enzymol. 76*, 72–87.
45. Light, W. R. (1987) Interactions of Heme with Apomyoglobin and Lipid Bilayers. Ph.D. Thesis, Rice University, Houston.
46. Irace, G., Balestrieri, C., Parlato, G., Servillo, L., and Colonna, G. (1981) Tryptophanyl fluorescence heterogeneity of apomyoglobins. Correlation with the presence of two distinct structural domains. *Biochemistry 20*, 792–799.
47. Tcherkasskaya, O., Bychkova, V. E., Uversky, V. N., and Gronenborn, A. M. (2000) Multisite fluorescence in proteins with multiple tryptophan residues. Apomyoglobin natural variants and site-directed mutants. *J. Biol. Chem. 275*, 36285–36294.
48. Tcherkasskaya, O., Ptitsyn, O. B., and Knutson, J. R. (2000) Nanosecond dynamics of tryptophans in different conformational states of apomyoglobin proteins. *Biochemistry 39*, 1879–1889.
49. Ervin, J., Larios, E., Osvath, S., Schulten, K., and Gruebele, M. (2002) What causes hyperfluorescence: Folding intermediates or conformationally flexible native states? *Biophys. J. 83*, 473–483.
50. Griko, Y. V., Privalov, P. L., Venyaminov, S. Y., and Kutyshenko, V. P. (1988) Thermodynamic study of the apomyoglobin structure. *J. Mol. Biol. 202*, 127–138.

51. Nishii, I., Kataoka, M., and Goto, Y. (1995) Thermodynamic stability of the molten globule states of apomyoglobin. *J. Mol. Biol. 250*, 223–238.
52. Barrick, D., and Baldwin, R. L. (1993) Stein and Moore Award address. The molten globule intermediate of apomyoglobin and the process of protein folding. *Protein Sci. 2*, 869–876.
53. Barrick, D., Hughson, F. M., and Baldwin, R. L. (1994) Molecular mechanisms of acid denaturation. The role of histidine residues in the partial unfolding of apomyoglobin. *J. Mol. Biol. 237*, 588–601.
54. Liong, E. C., Dou, Y., Scott, E. E., Olson, J. S., and Phillips, G. N., Jr. (2001) Waterproofing the heme pocket. Role of proximal amino acid side chains in preventing hemin loss from myoglobin. *J. Biol. Chem. 276*, 9093–9100.
55. Wittung-Stafshede, P., Malmstrom, B. G., Winkler, J. R., and Gray, H. B. (1998) Folding of deoxymyoglobin triggered by electron transfer. *J. Phys. Chem. 102*, 5599–5601.
56. Hughson, F. M., Barrick, D., and Baldwin, R. L. (1991) Probing the stability of a partly folded apomyoglobin intermediate by site-directed mutagenesis. *Biochemistry 30*, 4113–4118.
57. Marden, M. C., Hazard, E. S., Leclerc, L., and Gibson, Q. H. (1989) Flash photolysis of the serum albumin-heme-CO complex. *Biochemistry 28*, 4422–4426.